High-Frequency Linear Array (20 MHz) based on Lead-Free BCTZ Crystal

Claire Bantignies, R. Rouffaud, Gabriel Buse, P. Veber, Hugues Cabane, Ana Borta-Boyon, Mai Pham Thi, Pascal Mauchamp, A. Lejeune, Mario Maglione, et al.

High-Frequency Linear Array (20 MHz) based on Lead-Free BCTZ Crystal

C. Bantignies, R. Rouffaud, G. Buse, P. Veber, H. Cabane, A. Borta-Boyon, M. Pham Thi, P. Mauchamp, A. Lejeune, M. Maglione, L. Colin, A. Balé, M. Flesch, F. Levassort, *Member, IEEE.*

***Abstract*— Centimeter-sized $BaTiO_3$-based crystals grown by top-seeded solution growth from the $BaTiO_3$−$CaTiO_3$−$BaZrO_3$ system were used to process a high-frequency (HF) lead-free linear array. Piezoelectric plates with $(110)_{pc}$ cut within 1° accuracy were used to manufacture two 1-3 piezo-composites with thicknesses of 270 and 78 μm for resonant frequencies in air of 10 and 30 MHz, respectively. The electromechanical characterization of the BCTZ crystal plates and the 10 MHz piezocomposite yielded thickness coupling factors of 40% and 50%, respectively. We quantified the electromechanical performance of the second piezocomposite (30 MHz) according to the reduction in the pillar sizes during the fabrication process. The dimensions of the piezocomposite at 30 MHz were sufficient for a 128-element array with a 70 μm element pitch and a 1.5 mm elevation aperture. The transducer stack (backing, matching layers, lens and electrical components) was tuned with the characteristics of the lead-free materials to deliver optimal bandwidth and sensitivity. The probe was connected to a real-time HF 128-channel echographic system for acoustic characterization (electroacoustic response, radiation pattern) and to acquire high-resolution *in vivo* images of human skin. The center frequency of the experimental probe was 20 MHz, and the fractional bandwidth at -6 dB was 41%. Skin images were compared against those obtained with a lead-based 20-MHz commercial imaging probe. Despite significant differences in sensitivity between elements, *in vivo* images obtained with a BCTZ-based probe convincingly demonstrated the potential of integrating this piezoelectric material in an imaging probe.**

***Index Terms*— High-frequency ultrasonic transducer, lead-free material, linear array, piezoelectricity, ultrasonic imaging.**

I. Introduction

Since Saito's work on the development of new lead-free piezoelectric materials with very good electromechanical performance [1], the interest shown by the international scientific community has continued to grow. This impetus is driven in part by a series of directives regulating the use of lead in commercial products within the jurisdiction, in particular, of the European Union [2]. Confirmed by an increasing number of publications in this field [3], [4], research activity has also led to review articles and monographs over the last 6 years, with special attention given to the perspectives and applications of lead-free compositions [3]–[10]. Among these applications, ultrasonic transducers specifically for medical imaging applications [11]–[13] represent an important stake with regard to economic issues.

Two of the most important material properties for these transducer applications are the effective electromechanical coupling coefficient (k) of the main vibration modes of the piezoelectric element and its acoustic impedance (Z) [14]. The k factor should be maximized and depends on the element's geometry. The thickness coupling factor (k_t) is considered for large plates or disks, while factor k_{33} is considered for pillars, and this factor is retained to evaluate the 1-3 piezocomposite [15], [16]. Similarly, Z should be as close as possible to that recorded on biological tissues (i.e., 1.5 MRayl). Additionally, the relative dielectric permittivity ($\varepsilon_{33}^S/\varepsilon_0$) plays a critical role in the electrical matching of the entire transducer to cables and electronics, although integrated electronics can currently limit the latter consideration.

Compiled from previous specifications, two plots of k_t and $\varepsilon_{33}^S/\varepsilon_0$ versus the acoustic impedance (Z) are shown in Fig. 1 for lead-free compositions. Similar plots were previously published [14], [17] for lead-based compositions. While many material parameters can/are extracted from publications on lead-free compositions, we have deliberately limited ourselves

Manuscript submitted xxx; accepted xxxx. This work was supported by the French Research Agency through the "High Efficiency Piezoelectric Alternative Materials: Towards Environmentally-Friendly Solutions" Project under Grant ANR 14-CE07-0028-01.

C. Bantignies (e-mail: c.bantignies@vermon.com), P. Mauchamp, A. Lejeune, M. Flesch are with VERMON SA, Tours, France

F. Levassort, R. Rouffaud, L. Colin, A. Balé are with the GREMAN UMR 7347, Université de Tours, CNRS, INSA CVL, Tours, France.

G. Buse is with Institute for Advanced Environmental Research (ICAM), West University of Timisoara, Romania.

P. Veber is with Université Lyon, Institut Lumière Matière UMR 5306, CNRS, Villeurbanne, France.

H. Cabane is with EZUS - CristalInnov, Sainte Hélène-du-Lac, France

A. Borta-Boyon and M. PhamThi are with Thales Research and Technology, Palaiseau, France

M. Maglione is with CNRS, Université de Bordeaux, ICMCB, UMR 5026, France

to materials used only for transducer fabrication (k_t, $\varepsilon_{33}^S/\varepsilon_0$, and Z values were available or easily deduced). Although this compilation is not exhaustive, we believe it is sufficiently representative. We have also chosen to divide these selected data into three main families that include certain variants such as composite or textured compositions: $(K,Na)NbO_3$ (KNN)-based in black, $Bi_{1/2}Na_{1/2}TiO_3$ (BNT)-based in blue and $BaTiO_3$ (BT)-based in orange. $LiNbO_3$ (LN) in purple and polymers/copolymers (PVDF/P(VDF-TrFE) in green) were also included. The main represented materials are ceramics (circled symbol) and single crystals (filled symbol). A central dot is added to the symbol to denote 1-3 piezocomposites (with ceramics or single crystals with inverted colors). Several commercial lead-free compositions are available with data sheets and denoted with a cross in the symbol.

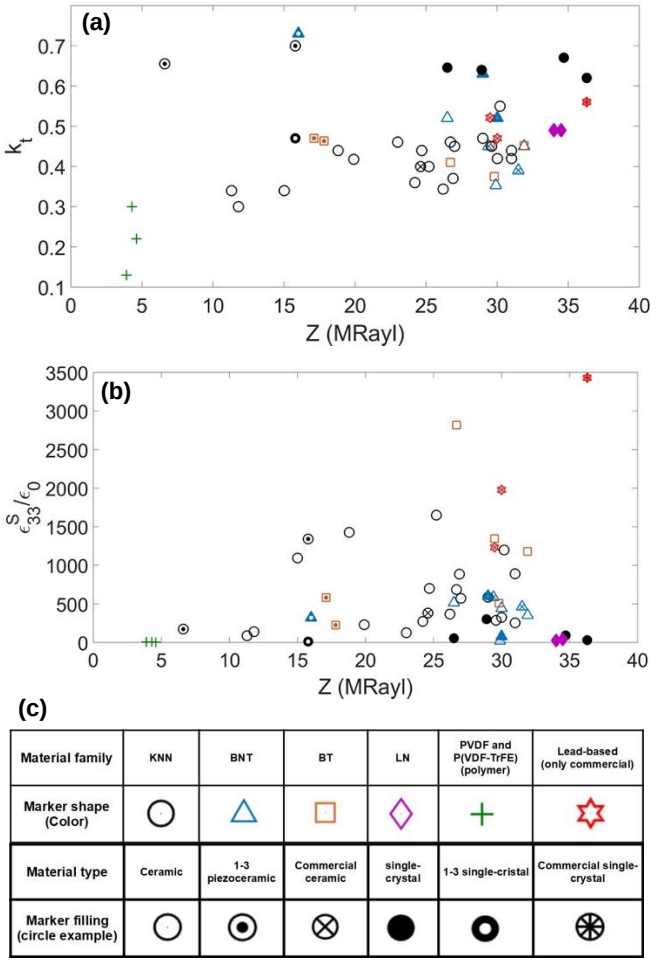

Fig. 1. (a) Thickness coupling factor (k_t) and (b) dielectric permittivity at constant strain ($\varepsilon_{33}^S/\varepsilon_0$) as a function of the acoustic impedance (Z) for lead-free piezoelectric materials (organized by families) used for transducer fabrication. (c) Description of symbols used (colors and shapes for material families; marker filling for material types).

Finally, only three commercial lead-based materials (two $Pb(Zr,Ti)O_3$ (PZT) ceramics [18], [19] and one $PbMg_{1/3}Nb_{2/3}O_3$-$PbTiO_3$ (PMN-PT) single crystal with mean properties [20]) were superimposed (in red) for comparison. These notations are summarized in Fig. 1c.

A wide range of acoustic impedance is observed for KNN-based ceramics, mainly due to the different porosity contents which make densification difficult for these compositions [21]–[35]. The fabrication process also has an influence (bulk ceramic, thick film, sintering, etc.). Globally, k_t tends to increase with increasing acoustic impedance (Z). For the dielectric permittivity at constant strain ($\varepsilon_{33}^S/\varepsilon_0$), a wide range of values is observed (until 1500) depending on the porosity content and dopants used. For KNN-based single crystals [36]–[38], k_t is improved between 60% and 70% and is accompanied by higher acoustic impedance values, mainly due to a higher longitudinal wave velocity than that in ceramics. Moreover, 1-3 piezocomposites based on single crystals [39] and ceramics [33] provide a better trade-off between k_t (70%, [40]) and Z, with performances that are comparable to those of soft PZT compositions.

For BNT-based compositions in single-crystal form [41], [42], k_t is significantly improved compared to ceramics at similar compositions [27], [43]–[45]. In the 1-3 configuration, good performance with a k_t over 70% is specified [42].
Here, additional data from two European companies with KNN-(Pz61)[46] and BNT-based materials (PIC 700 and PIC 701) [47] are mentioned.

For BT-based ceramics, the range of k_t is the same as that for previous compositions [48]–[50], and one ceramic composition with a high dielectric constant is identified [51]. Here, for the 1-3 piezocomposite (ceramic-based), acoustic impedance decreases with the use of polymer, which is expected. However, k_t is not significantly improved in this family, mainly due to the limited values of k_{33} [49], [50].

The lithium niobate crystal (LN) (36° rotated Y-cut) exhibits a good k_t (49%) with a much lower dielectric constant (approximately 30) [11], [52]. Finally, piezoelectric polymers often have lower k_t values (PVDF [52]), but they can still reach 30% for copolymers (P(VDF-TrFE) [53], [54]). These materials have low acoustic impedances and thus good acoustic matching with the propagation medium, which suits our imaging applications. These materials are readily available as thin, flexible sheets (i.e., a few tens of micrometers) and are generally well suited for the fabrication of HF transducers [55]. Among all the data presented here, more than half of the manufactured transducers, including the lead-free piezoelectric materials, are for HF applications (>20 MHz) and mostly exhibit a single-element configuration (90%). Within the three families (KNN-, BNT-, and BT-based) in this classification, KNN-based compositions are mainly studied and used for transducer applications.

The use of lead-free materials to manufacture multielement transducers is rare [26], [39], [42]. HF linear arrays with a large number of elements (typically 128) and a center frequency up to 40 MHz were fabricated [56]–[58]. Among these transducers, novel lead-free materials [36] were successfully integrated in this type of imaging probe.

In the present work, we proposed to evaluate materials from the BT-based family integrated into a HF linear array. The $(1-x)BaTi_{0.8}Zr_{0.2}O_3$-$xBa_{0.7}Ca_{0.3}TiO_3$ (BCTZ) solid solution showed a very high piezoelectric coefficient with a d_{33} up to 620 pC/N [6], [59]–[61]. As shown in Fig. 1 for the different families, the electromechanical properties are improved for single crystals compared to ceramics with similar compositions and are even higher for 1-3 piezocomposites. Piezoelectric

coefficients up to 1500-2000 pC/N are predicted [60] for BCTZ single crystals, making them interesting candidates for ultrasonic probes.

In section II, BCTZ material synthesis is briefly described, with particular attention given to synthesizing cm-sized crystals for our application. The microstructural characterization and functional property evaluation of the piezoelectric plates appear in Section II. Sections III and IV are devoted to the linear array fabrication with the 1-3 piezocomposite and acoustic characterization. Finally, images of human forearm skin obtained with the new ultrasonic probes are evaluated and compared with images obtained with a commercial lead-based probe.

II. Material Synthesis and Characterizations

A. Materials Synthesis

In this section, the main steps and characteristics of the BCTZ crystal growth process are summarized. The synthesis details can be found in [62]. Briefly, raw powders of $BaCO_3$, $CaCO_3$, TiO_2 and ZrO_2 (Fox Chemical GmbH, Pfinztal, Germany) were used for the synthesis of initial loads. The corresponding normalized composition of the initial liquid solution, with respect to the segregation of Ca and Zr, was the following (mol. %): Ba (88.7), Ca (11.3), Ti (98.7) and Zr (1.3). These values were used to cross the vicinity of the BCTZ50 composition given by Keeble *et al.* [59] and Liu *et al.* [60]. The solid-state reaction was first performed by thermal processing [63] in air using a platinum crucible. Then, top-seeded solution growth (TSSG) [64] was used to grow crystals in iridium crucibles (80*80 mm^2) in an induction furnace operating under a controlled argon atmosphere. Crystallization was seeded using a 2 mm-diameter iridium rod at a rotational speed of 0.5 rpm. Crystal growth occurred at a saturation temperature range of approximately [1485-1570]°C, and the bulk single crystal was cooled over a 48 h duration. These parameters were optimized to avoid unwanted shapes (typically spiral shapes) and to obtain a crystal with a cylindrical shape (diameter of 50 mm and a weight of 330 g) [62][Fig. 2(a)]. This process resulted in the successful extraction of boule-oriented and centimeter-sized crystals. Crystals in the $(110)_{pc}$ direction were oriented and cut within 1° of accuracy [Fig. 2(b)]. The sample was poled in air with an increasing electric field up to 1 kV/mm at room temperature.

B. Material characterization

Electron probe microanalysis (EPMA, CAMECA SX-100, Gennevilliers, France) was used to characterize several samples at different positions in the bulk single crystal, and variations in Zr and Ca contents were determined. Specifically, the Zr content decreased while the Ca content increased as a function of the radius and height, with periodical fluctuations down to +/- 2 mol % and +/- 5 mol % for the Ca and Zr contents, respectively.

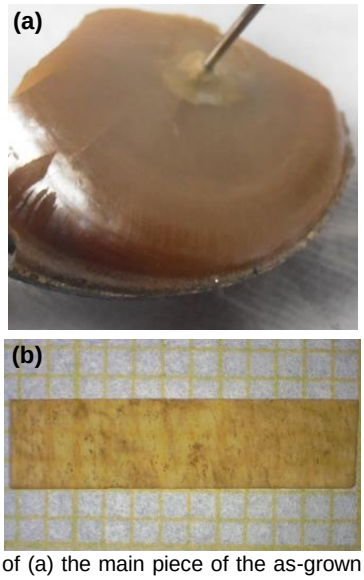

Fig. 2. Pictures of (a) the main piece of the as-grown crystal, partially fractured during extraction, with original cylindrical shape (approximately 50 mm in diameter) (b) centimeter-sized sample extracted from this bulk single crystal and oriented along the $(110)_{pc}$ direction (one square represents 1 mm^2).

These fluctuations were complementary, i.e., locally, a minimum content of Ca corresponded to a maximum content of Zr and *vice versa*. The presence of two solid solutions with extreme compositions in the entire boule explains these fluctuations [62]. For our selected samples, the measured average composition was $(Ba_{0.905}Ca_{0.095})(Ti_{0.943}Zr_{0.057})$ over 50 points, with ±0.003 accuracy. The direct piezoelectric coefficient, d_{33}, was measured at room temperature with a Berlincourt d_{33} meter (APC International Ltd., Mill Hall, PA, USA) and delivered a value of 208 pC/N. Measurement of the dielectric constant at 1 kHz of the poled sample as a function of the temperature gives a tetragonal-cubic transition (Curie temperature, T_c) at 106 °C in agreement with the chemical content and orthorhombic-tetragonal phase transition ($T_{0\text{-}T}$) at approximately 0 °C.

TABLE I
FUNCTIONAL PROPERTIES OF THE PIEZOELECTRIC SAMPLES

	Plate	1-3 LF	1-3 HF
t (μm)	590	270	78
A (mm^2)	232	31	12.3
v_f (%)	100	60	65
ρ (kg/m^3)	5485	3700	3950
k_t (%)	42.8	50.6	35
$\varepsilon_{33}^S/\varepsilon_0$	1190	810	530
δ_m (%)	8.9	19	14
δe (%)	1.5	1.5	4.8
Z (MRayl)	37.3	19.0	22.7
f_o (MHz)	5.7	9.8	31.0

t: thickness; A: area of the electrodes; v_f: piezoelectric BCTZ volume fraction; ρ: density; k_t: thickness coupling factor; $\varepsilon_{33}^S/\varepsilon_0$: dielectric permittivity at constant strain; δ_m: mechanical loss factor; δ_e: dielectric loss factor; Z: acoustic impedance; f_0: resonant frequency in air.

For the electromechanical characterization, an HP4395A network analyzer (Agilent Technologies Inc., Palo Alto, CA) and the corresponding impedance test kit were used to measure electrical impedance as a function of the frequency of samples placed under free piezoelectric resonator conditions [Figs. 3(a) 3(b) and 3(c)]. A KLM-equivalent electrical circuit [65], [66] was employed to compute the theoretical behavior of the electrical impedance. A fitting process led to the thickness-mode parameters of the piezoelectric samples. The functional properties of the characterized BCTZ crystal plate with dimensions of 30.1×7.5×0.59 mm^3 are summarized in Table I (column "plate"). A k_t value of approximately 43% falls in the same range as those of other BT-based compositions (ceramics) [49].

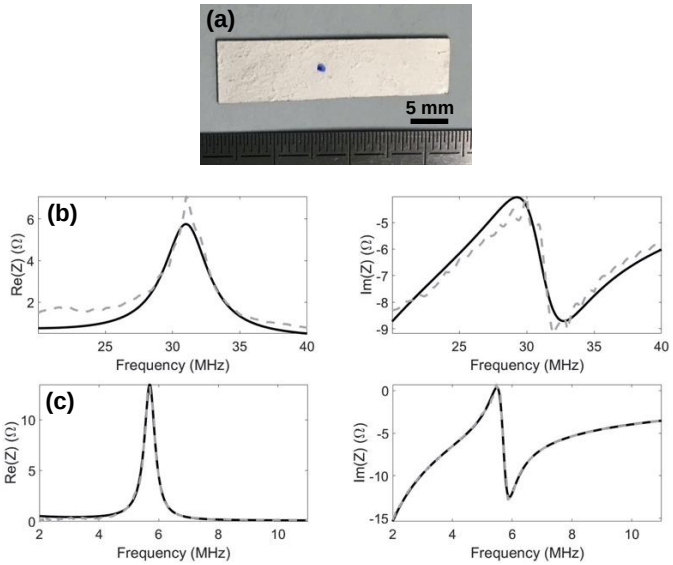

Fig. 3. (a) Picture of the BCTZ crystal plate with a silver paste electrode in air. Real (Re(Z)) and imaginary (Im(Z)) parts (solid black lines: theoretical; gray dashed lines: experimental values) of the complex electrical impedance Z of (b) 1-3HF composite in air and (c) BCTZ crystal plate with electrode in air.

III. HF LINEAR ARRAY FABRICATION

A. 1-3 Piezocomposites

The BCTZ crystal plate was first polished to slightly reduce the thickness while maintaining good flatness. Two 1-3 piezocomposites were fabricated for electromechanical property measurements. The first was fabricated to evaluate the BCTZ material in this 1-3 configuration and had a resonant frequency of 10 MHz. This property allowed the use of relatively large pitches (90 µm) considering the standard requirements for minimizing lateral modes of vibration (i.e., with an aspect ratio (AR) height/width of BCTZ pillars to be at least 3 in the ideal case) [67]–[69]. The second sample was fabricated and integrated in a linear array, which necessitated a thickness reduction to reach a resonance frequency in air of approximately 30 MHz. In this case, the pitch was also significantly reduced with a homothetic rule to maintain an AR of approximately 3 (pitch approximately 40 µm). The dice-and-fill method [70] was applied to fabricate 1-3 piezocomposites. BCTZ volume fractions for both samples were close [60% for 1-3 low-frequency (1-3LF) and 65% for 1-3 high-frequency (1-3HF) samples]. The Smith physical model [16] was used to simulate effective parameters, such as k_t, $\varepsilon_{33}^S/\varepsilon_0$ and Z, as a function of the piezoelectric phase volume fraction and to identify favorable trade-offs to deduce these volume fractions regarding the characteristics of the resin (Epo-Tek 301, Epoxy Technology, Billerica, MA, USA). Simulations were similarly undertaken before for the PMN-PT single crystal to define a real benchmark, and a similar composite structure was used for the BCTZ crystal. The corresponding mechanical properties differed from those of conventional lead-based single crystals, and the dicing conditions needed to be finely tuned due in particular to their rather greater fragility. The kerfs were filled with low viscosity epoxy resin (see Fig. 4 for the 1-3LF sample). After curing the hard epoxy resin, the samples were lapped to eliminate the excess polymer of the top face and the BCTZ substrate on the bottom face. This machining step allowed the sample to finally reach the desired thickness. Gold electrodes (100 nm) were sputtered on both faces of each sample, and they were poled again in air at room temperature. Electromechanical properties were determined using the same measurement procedures previously used for the BCTZ plate. Table I summarizes the results obtained. For the 1-3LF sample, k_t significantly improved (from 42.8 to 50.6%) compared to that recorded for the initial plate.

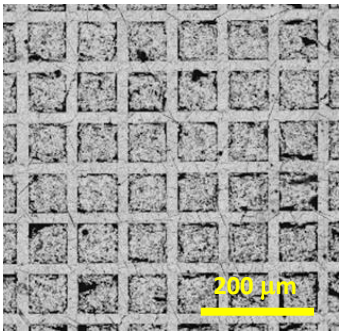

Fig. 4. SEM image of the BCTZ/epoxy 1-3 composite (1-3LF).

For the second 1-3HF sample, the electromechanical properties recorded decreased (k_t=35%). This decrease was mainly due to the machining process at the small scale with small pillar dimensions and the thickness size dependence of electromechanical properties [71]. We observed that both the dielectric permittivity and losses changed beyond a lower value of k_t, which confirmed this hypothesis. Despite these new performances, the reduction of the acoustic impedance remains an asset for the manufacture of the probe.

B. Fabrication

Another sample comparable to 1-3HF was manufactured and used to fabricate a 128-element probe. This sample has the same thickness and adapted lateral dimensions to integrate the entire surface area of all 128 elements. The elements were appropriately separated on one side (partial cut - not made over the full thickness of the piezoelectric composite by a dicing step performed with a diamond disk) with a pitch of 70 micrometers. The electrical contacts on each of these elements relied on a flexible circuit positioned at the array's pitch. A backing

material was then bonded on the flexible circuit to ensure structural rigidity. The acoustic head also consisted of two matching layers. The acoustic properties (quarter-wavelength thickness, acoustic impedance and low acoustic attenuation) of these two matching layers were deduced (in pulse mode [72]) using the Desilets relationship for the optimization of acoustic-energy transfer to the propagation medium. These layers with thicknesses of approximately 25 microns were fabricated and glued to the front face of the piezoelectric composite. The two layers were fabricated with a polymer loaded with submicron size metallic powder, for which the corresponding volume fractions were chosen to achieve the desired acoustic impedances. A silicon lens was molded on the top of the acoustic stack, which focused the ultrasound beam at approximately 8 mm and ensured encapsulation (Fig. 5).

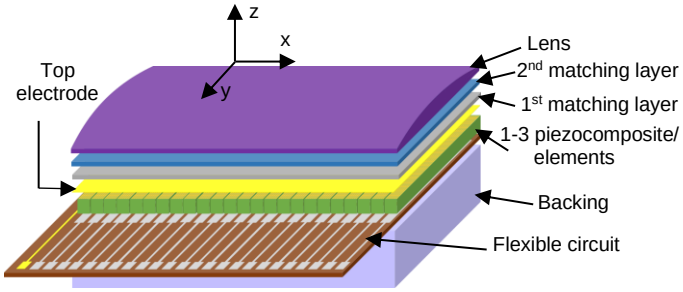

Fig. 5. Scheme of the acoustic stack of the BCTZ probe head.

This acoustic head was integrated into the probe housing and interconnected to a 2-meter coaxial cable with an electrical impedance of 80 Ohms. Finally, a HF interface connector dedicated to a Verasonic Vantage Platform (Verasonics, Redmond, WA, USA) was used (Fig. 6).

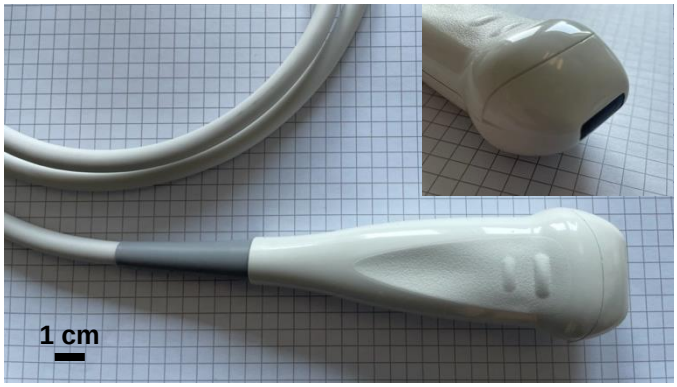

Fig. 6. Photograph of the imaging probe. Inset shows the top view of the imaging probe.

IV. Linear Array Characterization

We measured the pulse-echo response of a representative element (#75). A metallic plane target (aluminum) was placed 6.3 mm in front of the probe in a water-filled tank. The normalized corresponding frequency response was deduced and is shown in Fig. 7(a). The input signal consisted of a half-sinusoid cycle at 20 MHz frequency and a 25 V amplitude. These measurements were compared to simulation predictions from the KLM scheme [65] with the same electrical excitation signal, both for a single element in emission/reception with similar dimensions [Fig. 7(b)].

Our simulations considered all layers described in the stack Fig. 5. For this 1-D model, the acoustical impedance of the lens was very close to that recorded for water and was assumed to propagate through the medium without significant behavioral change. For each inert layer, the density, longitudinal wave velocity, and acoustic attenuation at 20 MHz were employed, while (1-3 HF) data shown in Table 1 were used for HF piezoelectric element simulations. The connecting cable used with a length of 2 m was also considered as a transmission line (quadrupole in the KLM scheme) where losses are neglected. Its impact on the properties of the theoretical electroacoustic response is weak. For this element, the center frequency was slightly lower than 20 MHz (precisely 18 MHz), and the fractional bandwidth at -6 dB was 44%. Regarding the theoretical results, the center frequency was comparable at 21 MHz, while a slight difference (2%) was observed for the fractional bandwidth at -6 dB (46%) with the KLM model.

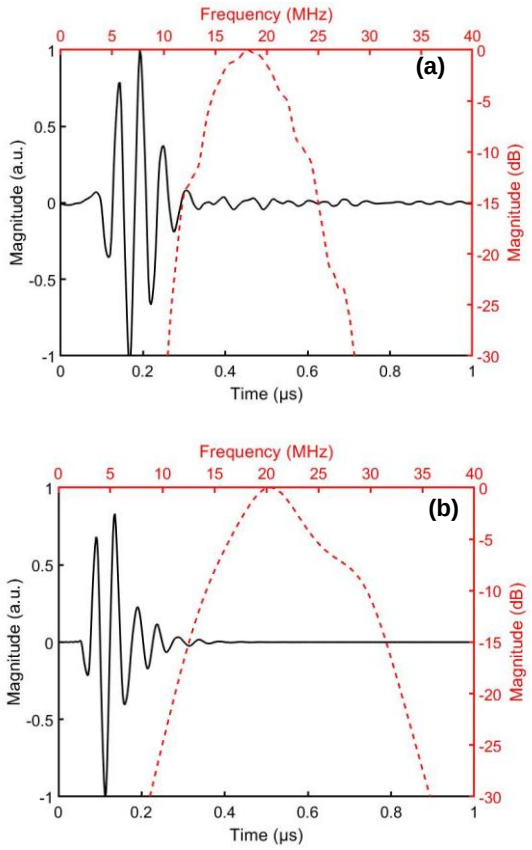

Fig. 7. (a) Normalized measured (element #75) and (b) simulated pulse echo response (black, solid lines) of one representative array element and its corresponding frequency responses (red, dashed lines).

The significant resonant center frequency difference between the composite in air and one representative element of the probe primarily originates from the flexible circuit. This decrease is observed on the theoretical electroacoustic response calculated with the KLM scheme. Taking into account the flex with a polymer layer of 20 μm and two copper electrodes of 4 μm thick (with an acoustic impedance higher than 40 MRayl), the center frequency decreases from 28 to 20 MHz. The

addition of the backing and the two matching layer also contributes to this decrease of frequency, but this contribution is less important.

Based on the electroacoustic response of this element (#75), the axial resolution was 170 μm (calculated from the width at half height of the signal envelope). All 128 elements were tested using the same procedure and yielded mean values of 20 MHz and 41% for the center frequency and fractional bandwidth, respectively. Fig. 8 shows the relative sensitivity values of each element (normalized with the mean sensitivity value), as deduced from these measurements. Two (#69 and #112) of these elements were defective. The variation in sensitivity was relatively large, with a maximum difference of approximately 30 dB. Presumably, this difference was due to the nonuniformity of the electromechanical performance of the 1-3HF composite for each element. Indeed, during the manufacturing process of the 1-3 piezocomposite, several pillars broke or cracked, as observed on several SEM images (Fig. 4). The number of rows of pillars on the width of the elements of the probe is low (around 3), which can lead to a rapid degradation of the performance of the element overall. Although the cutting parameters have already been modified from those used for lead-based compositions, additional studies, such as studies of the cutting speed or the choice of the diamond blade for the dice-and-fill method, remain necessary.

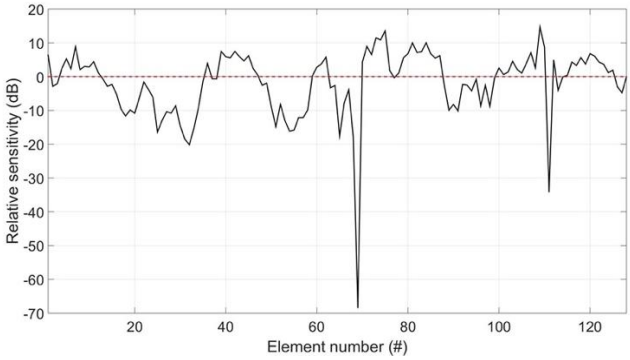

Fig. 8. Measured relative sensitivity of all 128 elements (red dashed line is the mean value for normalization at 0 dB).

Radiation patterns were evaluated in water using a capsule hydrophone (Onda, HGL-0085, Sunnyvale, CA, USA) with an aperture of 85 μm. The test hydrophone was connected to a preamplifier with a 20 dB gain, and the corresponding signals were viewed on an oscilloscope (Teledyne Lecroy, HDO4034A, Chestnut Ridge, NY, USA). The input signal consisted of 5 cycles at the center frequency of the probe with an amplitude of 50 Vpp. Measurements involved scanning several (x-y) planes (see Fig. 5 for axis description) (each 100 μm in both directions) at depths (z-axis) between 0.1 and 13 mm (each 200 μm). The selected configuration used 49 elements centered on element #40 and an f-number (f#=2.0). Variations in the sensitivity between elements had a nonnegligible effect on the radiation pattern, as shown in Figs. 9(a) and 9(c). The measured focal distance was approximately 7 mm, while the lateral width at -3 dB and 265 μm was significantly modified compared to what one can compute with the standard relation (λ x f# = 165 μm). The MATLAB toolbox (Mathwork, Natik, MA, USA) discrete representation array modeling (DREAM) [73] was used to simulate this radiation pattern. To this end, the characteristics of the chosen input acceleration signals for each element were identical to those of the pulse echo response (Fig. 7(a) with the same center frequency and bandwidth) and set of measured relative sensitivities given in Fig. 8 considered for all 49 elements. All maximum amplitude accelerations were adjusted with an identical ratio for all elements to obtain similar pressure values at the focal point for the experimental results and simulation (115 kPa). These results are shown in Fig. 9(b) and exhibited similar behavior to that of the experimental material [Fig. 9(a)]. The lateral width at -3 dB was 335 μm. In both cases, the depth of field (-3 dB) was between 8 and 10 mm. Although these values are considered good, a cursory review of both figures shows that the spatial pressure distribution lacks localized concentration within the focal zone. This simulation highlights the major effects of the sensitivity variations. To confirm this finding, the DREAM MATLAB toolbox [73] was used to simulate the radiation pattern considering that all the elements had a sensitivity identical to that of element #75, as shown in Fig. 9(c). In this idealized case, both the deduced lateral width at -3 dB (140 μm) and sensitivity in the focal zone for a depth of field of 2.6 mm improved. Similarly, between the two simulations, a 5 dB gain was obtained at the focal point [Fig. 9(b) and Fig. 9(c)].

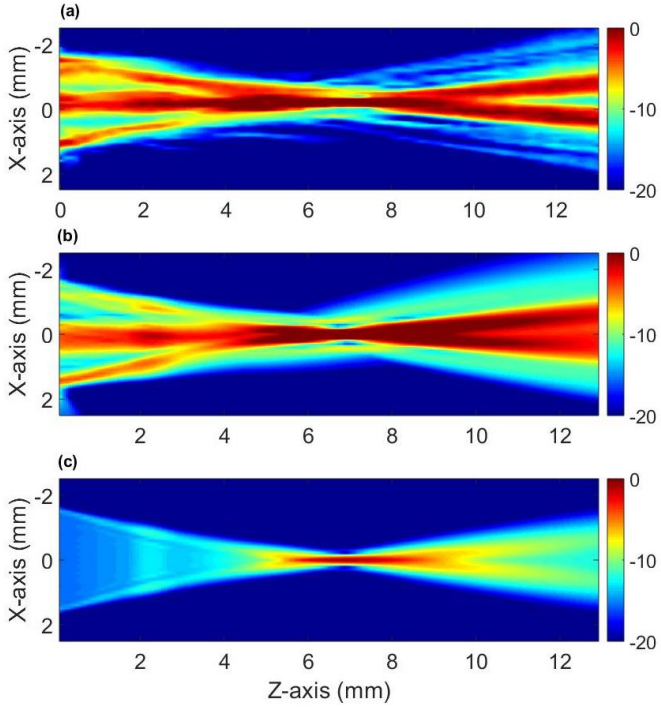

Fig. 9. Radiation pattern (normalized pressure at the focal point at 0 dB) of the linear array: (a) experimental; (b) simulation taking into account the sensitivity variation between elements as given in Fig. 6; (c) simulation with the same sensitivity for all the elements (element #75 as reference).

The transducer was subjected to additional experiments and images were acquired with a a 50-μm tungsten wire phantom. This wire was positioned at the focal distance (7 mm) in water and perpendicular to the acoustic beam of the transducer. The characteristics used to obtain the B-Mode image (Fig. 10) were the same as those described previously (49 element and

f#=2.0). Since the wire diameter is smaller than the wavelength, the lateral resolution (at −6 dB) could be measured [74] and was equal to 307 µm.

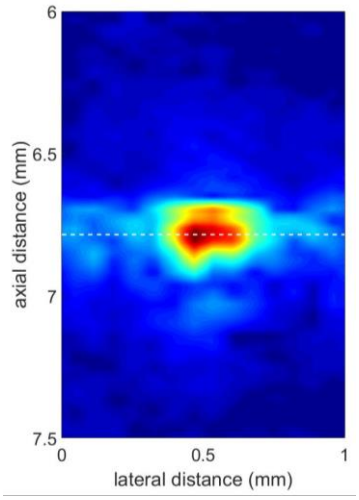

Fig. 10. Image of a 50-µm tungsten wire positioned at the measured focal distance (normalized amplitude).

V. Imaging Evaluation

This lead-free probe interfaced with the HF commercial ultrasound research Verasonic Vantage Platform (Verasonics, Redmond, WA, USA) was used for imaging evaluation. Linear scanning was performed using 49 elements in transmission and all 128 elements in reception. Here, a fixed focus was used in transmission with f#=2.0. Real-time, *in vivo* images of human forearm skin were acquired [Fig. 11(a)]. These images were compared to those obtained in the same area with a commercial piezoelectric single-crystal probe (L22-14vX, Verasonics [75]) with 128 elements, a center frequency of 18 MHz, and a pitch with a higher value at 100 µm. When the number of elements used in transmission was adapted [Fig. 11(b)], an identical f-number was used.

Previously, acoustic pressure delivered by one element at the surface for the two probes was measured with the following values: 1.5 kPa/V (element #75) and 6 kPa/V for lead-free and lead-based probes, respectively.

For both images, three main layers of the skin, namely, the epidermis, dermis and hypoechogenic hypodermis, were observed. Vessels and arteries with their inner wall were clearly distinguishable, confirming satisfactory spatial resolutions.
However, the lead-based probe had better sensitivity than the lead-free probe. Here, 6 dB more was used on the TGC (time gain compensation) for the image with the BCTZ-based probe, allowing us to observe the structures below the artery and vessels (beyond 9 mm). The pressure measured in these configurations at the focal point for both probes showed a difference of 12 dB. The lead-based imaging probe integrated a piezoelectric lead-based single crystal with a high coupling factor, which exhibited very good sensitivity. Moreover, the area element was significantly higher for the lead-based imaging probe, where the pitch was 100 µm (70 µm for the lead-free imaging probe) and the elevation was 2 mm (1.5 mm for the lead-free probe). Improving the manufacture of the 1-3 piezocomposite to obtain a more uniform structure should reduce the variation in the sensitivity between elements and thus to yield a radiation pattern more in line with the theoretical results.

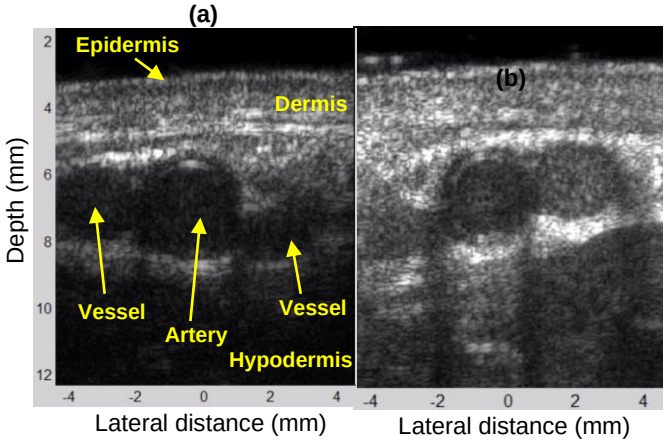

Fig. 11. Ultrasound images of human forearm skin acquired with (a) the BCTZ-based probe (20 MHz) and (b) the commercial L22-14vX lead-based probe (18 MHz).

VI. Conclusion

In the introductory section of this report, we reviewed the functional parameters of several lead-free piezoelectric materials commonly used to manufacture ultrasonic transducers. We observed that several HF transducers (typically between 20 and 50 MHz) have already been manufactured, at least on a laboratory scale. The KNN-based family of lead-free transducers is the most commonly used category for HF applications. Equally, substantial efforts were made in developing the lead-free barium titanate-based family, especially for ceramics, although $BaTiO_3$ was the first polycrystalline ceramic material known to exhibit ferroelectricity. In the present study, BCTZ crystals were used and, for the first time, fabricated in a 1-3 composite configuration and later integrated into a HF linear array. The first objective was to deliver a centimeter-sized plate for our targeted application. The electromechanical properties for our fabricated 1-3 piezocomposite were satisfactory. We recorded a thickness coupling factor exceeding 50% at 10 MHz, which decreased at a higher frequency (30 MHz), suggesting room for improvement for both the microstructure homogeneity and the machining conditions. A 128-element, HF linear array (20 MHz) was fabricated, characterized, and evaluated using a commercial ultrasound research platform. We set a reference based on *in vivo* image evaluations performed with a commercial lead-based single-crystal linear array with similar center frequency and similar numbers of elements. A difference in sensitivity, mainly due to a lower thickness coupling factor of the lead-free piezoelectric material and variation of this sensitivity between elements, was observed for the resulting images, but good spatial resolutions were retained. This lead-free probe remains fully operational. From an engineering point of view, this study covers a complete set of challenges, starting from new piezoelectric material fabrication to ultrasound images. This study shows that the integration of new lead-free

materials in transducers for medical imaging at the industrial scale is generally achievable. Nevertheless, several challenges remain to be addressed, namely upscaling, reproducibility, reliability, and leveraging the cost of piezoelectric materials, because the desired performances for some compositions should be comparable to those typical of lead-based piezomaterials We anticipate that the various points mentioned and corresponding advances can and are achievable in close collaboration between academic institutions and end users.

ACKNOWLEDGMENT

The authors would like to thank the French CERTeM Technological Platform for technological support. J.-M. Grégoire (UMR 1253, iBrain, Université de Tours; INSERM, France) is, thanked for his help in producing ultrasound images and Flavien Barcella for help in formatting this document.

REFERENCES

[1] Y. Saito *et al.*, "Lead-free piezoceramics," *Nature*, vol. 432, no. 7013, pp. 84–87, Nov. 2004, doi: 10.1038/nature03028.

[2] A. J. Bell and O. Deubzer, "Lead-free piezoelectrics—The environmental and regulatory issues," *MRS Bull.*, vol. 43, no. 8, pp. 581–587, Aug. 2018, doi: 10.1557/mrs.2018.154.

[3] J. Rödel, K. G. Webber, R. Dittmer, W. Jo, M. Kimura, and D. Damjanovic, "Transferring lead-free piezoelectric ceramics into application," *J. Eur. Ceram. Soc.*, vol. 35, no. 6, pp. 1659–1681, Jun. 2015, doi: 10.1016/j.jeurceramsoc.2014.12.013.

[4] J. Wu, D. Xiao, and J. Zhu, "Potassium–Sodium Niobate Lead-Free Piezoelectric Materials: Past, Present, and Future of Phase Boundaries," *Chem. Rev.*, vol. 115, no. 7, pp. 2559–2595, Apr. 2015, doi: 10.1021/cr5006809.

[5] C.-H. Hong *et al.*, "Lead-free piezoceramics – Where to move on?," *J. Materiomics*, vol. 2, no. 1, pp. 1–24, Mar. 2016, doi: 10.1016/j.jmat.2015.12.002.

[6] M. Acosta *et al.*, "$BaTiO_3$-based piezoelectrics: Fundamentals, current status, and perspectives," *Appl. Phys. Rev.*, vol. 4, no. 4, p. 041305, Dec. 2017, doi: 10.1063/1.4990046.

[7] T. Zheng, J. Wu, D. Xiao, and J. Zhu, "Recent development in lead-free perovskite piezoelectric bulk materials," *Prog. Mater. Sci.*, vol. 98, pp. 552–624, Oct. 2018, doi: 10.1016/j.pmatsci.2018.06.002.

[8] J. Koruza, A. J. Bell, T. Frömling, K. G. Webber, K. Wang, and J. Rödel, "Requirements for the transfer of lead-free piezoceramics into application," *J. Materiomics*, vol. 4, no. 1, pp. 13–26, Mar. 2018, doi: 10.1016/j.jmat.2018.02.001.

[9] H.-C. Thong *et al.*, "Technology transfer of lead-free (K, Na)NbO3-based piezoelectric ceramics," *Mater. Today*, vol. 29, pp. 37–48, Oct. 2019, doi: 10.1016/j.mattod.2019.04.016.

[10] J. Wu, *Advances in Lead-Free Piezoelectric Materials*. Singapore: Springer Singapore, 2018. doi: 10.1007/978-981-10-8998-5.

[11] Q. Zhou, K. H. Lam, H. Zheng, W. Qiu, and K. K. Shung, "Piezoelectric single crystal ultrasonic transducers for biomedical applications," *Prog. Mater. Sci.*, vol. 66, pp. 87–111, Oct. 2014, doi: 10.1016/j.pmatsci.2014.06.001.

[12] E. Taghaddos, M. Hejazi, and A. Safari, "Lead-free piezoelectric materials and ultrasonic transducers for medical imaging," *J. Adv. Dielectr.*, vol. 05, no. 02, p. 1530002, Jun. 2015, doi: 10.1142/S2010135X15300029.

[13] S. Garroni *et al.*, "Advanced Synthesis on Lead-Free $K_x Na_{(1-x)} NbO_3$ Piezoceramics for Medical Imaging Applications," *Phys. Status Solidi A*, vol. 215, no. 16, p. 1700896, Aug. 2018, doi: 10.1002/pssa.201700896.

[14] M. Lethiecq, F. Levassort, D. Certon, and L. P. Tran-Huu-Hue, "Piezoelectric Transducer Design for Medical Diagnosis and NDE," in *Piezoelectric and Acoustic Materials for Transducer Applications*, A. Safari and E. K. Akdoğan, Eds. Boston, MA: Springer US, 2008, pp. 191–215. doi: 10.1007/978-0-387-76540-2_10.

[15] R. E. Newnham, D. P. Skinner, and L. E. Cross, "Connectivity and piezoelectric-pyroelectric composites," *Mater. Res. Bull.*, vol. 13, no. 5, pp. 525–536, May 1978, doi: 10.1016/0025-5408(78)90161-7.

[16] W. A. Smith and B. A. Auld, "Modeling 1-3 composite piezoelectrics: thickness-mode oscillations," *IEEE Trans. Ultrason. Ferroelectr. Freq. Control*, vol. 38, no. 1, pp. 40–47, Jan. 1991, doi: 10.1109/58.67833.

[17] F. Levassort, L.-P. Tran-Huu-Huel, J._M. Gregoire, and M. Lethiecq, "High-frequency ultrasonic transducers-Fabrication, characterisation, performance," in *Material Technology and Design of Integrated Piezoelectric Devices*, Courmayeur-Italy, Feb. 2004, pp. 53–69. [Online]. Available: https://hal-univ-tours.archives-ouvertes.fr/hal-03343695

[18] "Data Sheet Pz21 MEGGITT Ferroperm Piezoceramics." https://www.meggittferroperm.com/wp-content/uploads/2017/10/Datasheet-very-soft-pz21.pdf

[19] "Data Sheet Pz27 MEGGITT Ferroperm Piezoceramics." https://www.meggittferroperm.com/wp-content/uploads/2017/10/Datasheet-soft-pz27.pdf

[20] "TRS Technologies." http://www.trstechnologies.com/Materials/High-Performance-PMN-PT-Piezoelectric-Single-Crystal

[21] X. Yan *et al.*, "Lead-free BNT composite film for high-frequency broadband ultrasonic transducer applications," *IEEE Trans. Ultrason. Ferroelectr. Freq. Control*, vol. 60, no. 7, pp. 1533–1537, Jul. 2013, doi: 10.1109/TUFFC.2013.2726.

[22] M.-R. Yang, S.-Y. Chu, and C.-C. Tsai, "An ultrasonic therapeutic transducers using lead-free Na0.5K0.5NbO3–CuNb2O6 ceramics," *J. Alloys Compd.*, vol. 507, no. 2, pp. 433–438, Oct. 2010, doi: 10.1016/j.jallcom.2010.07.150.

[23] D. W. Wu, R. M. Chen, Q. F. Zhou, K. K. Shung, D. M. Lin, and H. L. W. Chan, "Lead-free KNLNT piezoelectric ceramics for high-frequency ultrasonic transducer application," *Ultrasonics*, vol. 49, no. 3, pp. 395–398, Mar. 2009, doi: 10.1016/j.ultras.2008.11.003.

[24] D. W. Wu, R. M. Chen, Q. F. Zhou, D. M. Lin, H. L. W. Chan, and K. K. Shung, "Lead-Free Piezoelectric Ceramics for High-Frequency Ultrasound Transducers," in *2007 IEEE Ultrasonics Symposium Proceedings*, New York, NY, USA, Oct. 2007, pp. 2590–2593. doi: 10.1109/ULTSYM.2007.652.

[25] A. Safari, M. Abazari, K. Kerman, N. Marandian-Hagh, and E. K. Akdogan, "$(K_{0.44}, Na_{0.52}, Li_{0.04})(Nb_{0.84}, Ta_{0.10}, Sb_{0.06})O_3$ Ferroelectric Ceramics," *IEEE Trans. Ultrason. Ferroelectr. Freq. Control*, vol. 56, no. 8, pp. 1586–1594, Aug. 2009, doi: 10.1109/TUFFC.2009.1223.

[26] Z. Zhang *et al.*, "Development of a KNN Ceramic-Based Lead-Free Linear Array Ultrasonic Transducer," *IEEE Trans. Ultrason. Ferroelectr. Freq. Control*, vol. 65, no. 11, pp. 2113–2120, Nov. 2018, doi: 10.1109/TUFFC.2018.2868413.

[27] K. A. Snook, S. Zhang, and T. R. Shrout, "5D-2 Lead Free Piezoelectric Ceramics for Medical Ultrasound Transducers," in *2006 IEEE Ultrasonics Symposium*, Vancouver, BC, Canada, 2006, pp. 351–354. doi: 10.1109/ULTSYM.2006.99.

[28] G. Feuillard *et al.*, "Comparative performances of new KNN lead-free piezoelectric materials and classical lead-based ceramics for ultrasonic transducer applications," in *IEEE Symposium on Ultrasonics, 2003.*, Honululu, HI, USA, 2003, vol. 2, pp. 1995–1998. doi: 10.1109/ULTSYM.2003.1293308.

[29] M. Bah *et al.*, "Ultrasonic transducers based on undoped lead-free (K0.5Na0.5)NbO3 ceramics," *Ultrasonics*, vol. 63, pp. 23–30, Dec. 2015, doi: 10.1016/j.ultras.2015.06.007.

[30] G. Lévêque, P. Marchet, F. Levassort, L. P. Tran-Huu-Hue, and J. R. Duclere, "Lead free (Li,Na,K)(Nb,Ta,Sb)O3 piezoelectric ceramics: Influence of sintering atmosphere and ZrO2 doping on densification, microstructure and piezoelectric properties," *J. Eur. Ceram. Soc.*, vol. 31, no. 4, pp. 577–588, Apr. 2011, doi: 10.1016/j.jeurceramsoc.2010.10.031.

[31] F. Levassort, K. Astafiev, R. Lou-Moeller, J.-M. Grégoire, L. Nielsen, W.W. Wolny, M. Lethiecq, "Ultrasonic transducers based on curved lead-free piezoelectric thick films for high resolution medical imagin," Nantes, France, Apr. 2012, pp. 85–90. [Online]. Available: http://www.conforg.fr/acoustics2012/cdrom/data/articles/000405.pdf

[32] Z. Chen *et al.*, "High-Frequency Ultrasonic Imaging with Lead-free $(Na,K)(Nb,Ta)O_3$ Single Crystal," *Ultrason. Imaging*, vol. 39, no. 6, pp. 348–356, Nov. 2017, doi: 10.1177/0161734617701069.

[33] Z.-Y. Shen, J.-F. Li, R. Chen, Q. Zhou, and K. K. Shung, "Microscale 1-3-Type (Na,K)NbO3-Based Pb-Free Piezocomposites for High-

Frequency Ultrasonic Transducer Applications: Rapid Communications of the American Ceramic Society," *J. Am. Ceram. Soc.*, vol. 94, no. 5, pp. 1346–1349, May 2011, doi: 10.1111/j.1551-2916.2011.04508.x.

[34] J. Ou-Yang, B. Zhu, Y. Zhang, S. Chen, X. Yang, and W. Wei, "New KNN-based lead-free piezoelectric ceramic for high-frequency ultrasound transducer applications," *Appl. Phys. A*, vol. 118, no. 4, pp. 1177–1181, Mar. 2015, doi: 10.1007/s00339-015-9004-8.

[35] Y. Quan *et al.*, "Lead-Free KNN-Based Textured Ceramics for High-Frequency Ultrasonic Transducer Application," *IEEE Trans. Ultrason. Ferroelectr. Freq. Control*, vol. 68, no. 5, pp. 1979–1987, May 2021, doi: 10.1109/TUFFC.2020.3039120.

[36] R. Rouffaud, F. Levassort, M. Pham-Thi, E. Leveugle, and A.-C. Hladky-Hennion, "Electro-elastic moduli and frequency dependence of KN single crystal," in *Proceedings of ISAF-ECAPD-PFM 2012*, Aveiro, Portugal, Jul. 2012, pp. 1–4. doi: 10.1109/ISAF.2012.6297785.

[37] N. M. Kari, T. A. Ritter, S. E. Park, T. R. Shrout, and K. K. Shung, "Investigation of potassium niobate as an ultrasonic transducer material," in *2000 IEEE Ultrasonics Symposium. Proceedings. An International Symposium (Cat. No.00CH37121)*, San Juan, Puerto Rico, 2000, vol. 2, pp. 1065–1068. doi: 10.1109/ULTSYM.2000.921508.

[38] J. Ma *et al.*, "High frequency transducer for vessel imaging based on lead-free Mn-doped ($K_{0.44}Na_{0.56}$)NbO_3 single crystal," *Appl. Phys. Lett.*, vol. 111, no. 9, p. 092903, Aug. 2017, doi: 10.1063/1.4990072.

[39] C. Bantignies *et al.*, "Lead-free high-frequency linear-array transducer (30 MHz) for in vivo skin imaging," in *2013 IEEE International Ultrasonics Symposium (IUS)*, Prague, Czech Republic, Jul. 2013, pp. 785–788. doi: 10.1109/ULTSYM.2013.0202.

[40] Q. Ke, W. H. Liew, H. Tao, J. Wu, and K. Yao, "KNNS-BNZH Lead-Free 1–3 Piezoelectric Composite for Ultrasonic and Photoacoustic Imaging," *IEEE Trans. Ultrason. Ferroelectr. Freq. Control*, vol. 66, no. 8, pp. 1395–1401, Aug. 2019, doi: 10.1109/TUFFC.2019.2914464.

[41] Yan Chen, Xiang Ping Jiang, Hao Su Luo, Ji Yan Dai, and H. L. W. Chan, "High-frequency ultrasonic transducer fabricated with lead-free piezoelectric single crystal," *IEEE Trans. Ultrason. Ferroelectr. Freq. Control*, vol. 57, no. 11, pp. 2601–2604, Nov. 2010, doi: 10.1109/TUFFC.2010.1727.

[42] D. Zhou *et al.*, "Lead-free piezoelectric single crystal based 1–3 composites for ultrasonic transducer applications," *Sens. Actuators Phys.*, vol. 182, pp. 95–100, Aug. 2012, doi: 10.1016/j.sna.2012.05.030.

[43] M. M. Hejazi, B. Jadidian, and A. Safari, "Fabrication and evaluation of a single-element $Bi_{0.5}Na_{0.5}TiO_3$ -based ultrasonic transducer," *IEEE Trans. Ultrason. Ferroelectr. Freq. Control*, vol. 59, no. 8, pp. 1840–1847, Aug. 2012, doi: 10.1109/TUFFC.2012.2389.

[44] G. C. Edwards, S. H. Choy, H. L. W. Chan, D. A. Scott, and A. Batten, "Lead-free transducer for non-destructive evaluation," *Appl. Phys. A*, vol. 88, no. 1, pp. 209–215, May 2007, doi: 10.1007/s00339-007-3971-3.

[45] C. Fei *et al.*, "High Frequency Needle Ultrasonic Transducers Based on Lead-Free Co Doped Na0.5Bi4.5Ti4O15 Piezo-Ceramics," *Micromachines*, vol. 9, no. 6, p. 291, Jun. 2018, doi: 10.3390/mi9060291.

[46] "Data Sheet Pz61 MEGGITT Ferroperm Piezoceramics." https://www.meggittferroperm.com/wp-content/uploads/2017/11/MSSDK_PZ61_Datasheet-201711.pdf

[47] "Data sheet PIC700/PIC701 PI Ceramic." https://static.piceramic.com/fileadmin/user_upload/physik_instrumente/files/datasheets/PI_Ceramic_Material_Data.pdf

[48] S. T. F. Lee, K. H. Lam, X. M. Zhang, and H. L. W. Chan, "High-frequency ultrasonic transducer based on lead-free BSZT piezoceramics," *Ultrasonics*, vol. 51, no. 7, pp. 811–814, Oct. 2011, doi: 10.1016/j.ultras.2011.03.009.

[49] R. Ul, R. Rouffaud, L.-P. Tran-Huu-Hue, F. Levassort, M. Pham-Thi, and C. Bantignies, "Complete electroelastic set of co doped barium titanate for transducer applications," in *2017 IEEE International Ultrasonics Symposium (IUS)*, Washington, DC, Sep. 2017, pp. 1–4. doi: 10.1109/ULTSYM.2017.8092203.

[50] Y. Chen, K. Mei, C.-M. Wong, D. Lin, H. Chan, and J. Dai, "Ultrasonic Transducer Fabricated Using Lead-Free BFO-BTO+Mn Piezoelectric 1-3 Composite," *Actuators*, vol. 4, no. 2, pp. 127–134, May 2015, doi: 10.3390/act4020127.

[51] X. Yan *et al.*, "Correspondence: Lead-free intravascular ultrasound transducer using BZT-50BCT ceramics," *IEEE Trans. Ultrason. Ferroelectr. Freq. Control*, vol. 60, no. 6, pp. 1272–1276, Jun. 2013, doi: 10.1109/TUFFC.2013.2692.

[52] K. A. Snook *et al.*, "Design, fabrication, and evaluation of high frequency, single-element transducers incorporating different materials," *IEEE Trans. Ultrason. Ferroelectr. Freq. Control*, vol. 49, no. 2, pp. 169–176, Feb. 2002, doi: 10.1109/58.985701.

[53] J. S. Jeong and K. Kirk Shung, "Improved fabrication of focused single element P(VDF–TrFE) transducer for high frequency ultrasound applications," *Ultrasonics*, vol. 53, no. 2, pp. 455–458, Feb. 2013, doi: 10.1016/j.ultras.2012.08.013.

[54] A. Banquart *et al.*, "Piezoelectric P(VDF-TrFE) film inkjet printed on silicon for high-frequency ultrasound applications," *J. Appl. Phys.*, vol. 129, no. 19, p. 195107, May 2021, doi: 10.1063/5.0048444.

[55] F. S. Foster, K. A. Harasiewicz, and M. D. Sherar, "A history of medical and biological imaging with polyvinylidene fluoride (PVDF) transducers," *IEEE Trans. Ultrason. Ferroelectr. Freq. Control*, vol. 47, no. 6, pp. 1363–1371, Nov. 2000, doi: 10.1109/58.883525.

[56] S. Michau, P. Mauchamp, and R. Dufait, "Piezocomposite 30MHz linear array for medical imaging: design challenges and performances evaluation of a 128 elements array," in *2004 IEEE Ultrasonics Symposium Proceedings*, Montréal, Canada, pp. 898–901.

[57] C. Bantignies, P. Mauchamp, G. Ferin, S. Michau, and R. Dufait, "Focused 20 MHz single-crystal piezocomposite ultrasound array," in *2009 IEEE International Ultrasonics Symposium*, Rome, Sep. 2009, pp. 2722–2725. doi: 10.1109/ULTSYM.2009.5441566.

[58] C. Bantignies*et al.*, "40 MHz piezo-composite linear array and integration in a high resolution system," in *2011 IEEE International Ultrasonics Symposium*, Orlando, FL, Oct. 2011, pp. 226–229. doi: 10.1109/ULTSYM.2011.0055.

[59] D. S. Keeble, F. Benabdallah, P. A. Thomas, M. Maglione, and J. Kreisel, "Revised structural phase diagram of $(Ba_{0.7}Ca_{0.3}TiO_3)$-$(BaZr_{0.2}Ti_{0.8}O_3)$," *Appl. Phys. Lett.*, vol. 102, no. 9, p. 092903, Mar. 2013, doi: 10.1063/1.4793400.

[60] W. Liu and X. Ren, "Large Piezoelectric Effect in Pb-Free Ceramics," *Phys. Rev. Lett.*, vol. 103, no. 25, p. 257602, Dec. 2009, doi: 10.1103/PhysRevLett.103.257602.

[61] Y. Nahas *et al.*, "Microscopic origins of the large piezoelectricity of leadfree (Ba,Ca)(Zr,Ti)O3," *Nat. Commun.*, vol. 8, no. 1, p. 15944, Aug. 2017, doi: 10.1038/ncomms15944.

[62] G. Buse *et al.*, "Spinodal Decomposition in Lead-free Piezoelectric $BaTiO_3$–$CaTiO_3$–$BaZrO_3$ Crystals," *Cryst. Growth Des.*, vol. 18, no. 10, pp. 5874–5884, Oct. 2018, doi: 10.1021/acs.cgd.8b00596.

[63] F. Benabdallah, P. Veber, M. Prakasam, O. Viraphong, K. Shimamura, and M. Maglione, "Continuous cross-over from ferroelectric to relaxor state and piezoelectric properties of $BaTiO_3$ -$BaZrO_3$ -$CaTiO_3$ single crystals," *J. Appl. Phys.*, vol. 115, no. 14, p. 144102, Apr. 2014, doi: 10.1063/1.4870933.

[64] P. Veber, F. Benabdallah, H. Liu, G. Buse, M. Josse, and M. Maglione, "Growth and Characterization of Lead-free Piezoelectric Single Crystals," *Materials*, vol. 8, no. 11, pp. 7962–7978, Nov. 2015, doi: 10.3390/ma8115436.

[65] R. Krimholtz, D. A. Leedom, and G. L. Matthaei, "New equivalent circuits for elementary piezoelectric transducers," *Electron. Lett.*, vol. 6, no. 13, p. 398, 1970, doi: 10.1049/el:19700280.

[66] M. Lethiecq, F. Patat, L. Pourcelot, and L. P. Tran-Huu-Hue, "Measurement of losses in five piezoelectric ceramics between 2 and 50 MHz," *IEEE Trans. Ultrason. Ferroelectr. Freq. Control*, vol. 40, no. 3, pp. 232–237, May 1993, doi: 10.1109/58.216836.

[67] J. A. Hossack and G. Hayward, "Finite-element analysis of 1-3 composite transducers," *IEEE Trans. Ultrason. Ferroelectr. Freq. Control*, vol. 38, no. 6, pp. 618–629, Nov. 1991, doi: 10.1109/58.108860.

[68] A. Hladky-Hennion and J. Decarpigny, "Finite element modeling of active periodic structures: Application to 1–3 piezocomposites [a]," *J. Acoust. Soc. Am.*, vol. 94, no. 2, pp. 621–635, Aug. 1993, doi: 10.1121/1.406878.

[69] G. Hayward and J. Bennett, "Assessing the influence of pillar aspect ratio on the behavior of 1-3 connectivity composite transducers," *IEEE Trans. Ultrason. Ferroelectr. Freq. Control*, vol. 43, no. 1, pp. 98–108, Jan. 1996, doi: 10.1109/58.484469.

[70] H. P. Savakus, K. A. Klicker, and R. E. Newnham, "PZT-epoxy piezoelectric transducers: A simplified fabrication procedure," *Mater. Res. Bull.*, vol. 16, no. 6, pp. 677–680, Jun. 1981, doi: 10.1016/0025-

5408(81)90267-1.

[71] H. Dammak *et al.*, "Sample Thickness Dependence of Electromechanical Properties of PZN-PT and PMN-PT Single Crystals," in *2006 15th ieee international symposium on the applications of ferroelectrics*, Sunset Beach, NC, Jul. 2006, pp. 249–252. doi: 10.1109/ISAF.2006.4387878.

[72] C. S. Desilets, J. D. Fraser, and G. S. Kino, "The design of efficient broad-band piezoelectric transducers," *IEEE Trans. Sonics Ultrason.*, vol. 25, no. 3, pp. 115–125, May 1978, doi: 10.1109/T-SU.1978.31001.

[73] Lingvall Fredrik, "DREAM (Discrete REpresentation Array Modelling) Toolbox." Fredrik Lingvall (2021). DREAM (Discrete REpresentation Array Modelling) Toolbox (https://www.mathworks.com/matlabcentral/fileexchange/4502-dream-discrete-representation-array-modelling-toolbox), MATLAB Central File Exchange. Retrieved May 3, 2023. Available: https://www.mathworks.com/matlabcentral/fileexchange/4502-dream-discrete-representation-array-modelling-toolbox

[74] K. Raum and W. D. O'Brien, "Pulse-echo field distribution measurement technique for high-frequency ultrasound sources," *IEEE Trans. Ultra- son., Ferroelectr., Freq. Control*, vol. 44, no. 4, pp. 810–815, Jul. 1997, doi: 10.1109/58.655196.

[75] VERASONICS website, https://verasonics.com/wp-content/uploads/2020/10/datasheet_Vermon_probe_2020.pdf

Claire Bantignies was born in 1978 in Saint Quentin, France. She received a Master degree in materials science in 2001 at the University of Lille, France. She has been working at the VERMON Company, Tours, France in the R&D department in charge of process optimization for ultrasound transducers. She was also involved in R&D projects on the study of new active and passive materials for ultrasound devices.In 2014, she joined the new Advanced Research department in charge of new probe design, piezoelectric energy harvesting and lead-free material research. Since 2021, she is the leader of a team of 5 peoples in charge of the development of new processes in the Active Probe department.

Rémi Rouffaud was born in Saint-Yrieix-la-Perche, France, in 1987. He received the Diplome d'ingenieur degree in mechanical engineering in 2010, the M.Sc. degree in acoustics and vibrations from ENSIM, University of Le Mans, Le Mans, France, in 2010, and the Ph.D. degree from the University of Tours, Tours, France, in 2014. In 2015, he held a post-doctoral position at the Department of Biomedical Engineering, Federal University of Rio de Janeiro, Rio de Janeiro, Brazil. Since 2017, he has been with the GREMAN Laboratory, University of Tours, as an Associate Professor. His current research interests include ultrasonic transducers, piezoelectric materials, and the ultrasonic characterization of biological media.

Gabriel Buse is a Scientific Researcher at ICAM-West University of Timisoara. PhD thesis at WUT, Postdoc and Research Engineer in I.C.M.C.B. and Platform CristalInnov in France in the crystal growth and characterization domain. His experience includes numerous inorganic materials, ranging from simple oxides to fluorides obtained by Bridgman, Czochralski or Flux methods.

Philippe Veber works since 2001 in the fields of solid-state chemistry and the growth of bulk inorganic single crystals by various pulling methods from high temperature melts and solutions including Czochralski, Bridgman, zone levelling, micro-pulling down and flux techniques. He currently holds a permanent position as a Research Engineer at CNRS since 2007. After defending his Habilitation (HDR) in 2016 at University of Bordeaux, he is now assigned to the University Claude Bernard Lyon 1 since 2017. He is founder and member of the French Crystal Growth Committee belonging to the French scholarly Association of Crystallography. In addition, since 2020, he leads the national technology network CRISTECH-CNRS (500 members), which focuses on all crystallization processes of various compounds (inorganic, organic, molecular, biological). His own experience includes the growth of numerous inorganic dielectrics, ranging from simple oxides and fluorides to polycationic oxide materials dedicated, in particular, to optics, ferroelectricity and piezoelectricity.

Hugues Cabane received his PhD of Earth Sciences at University Blaise Pascal, Clermont-Ferrand, France, in 2002. Then he has been working for 20 years in the field of single crystals research and development, in Saint-Gobain Crystals and then in EZUS - Cristal Innov, since 2011. Piezoelectric crystals for sensors is one of his main current research interests.

Ana Borta-Boyon, photograph and biography not available at the time of publication.

Mai Pham Thi, photograph and biography not available at the time of publication.

Pascal Mauchamp, photograph and biography not available at the time of publication.

A Lejeune, photograph and biography not available at the time of publication.

Mario Maglione received the Ph.D. degree from the Federal Polytechnical School of Lausanne (EPFL), Lausanne, Switzerland (1987). Following three years PhD work with IBM Zürich Laboratories, Switzerland and post-doctoral positions with Mainz University, Germany, and IBM Zürich, he joined in 1988, as a Junior CNRS Scientist, the Physics Laboratory, University of Burgundy, Dijon, France. In 2000, he joined the CNRS Institute for Condensed Matter Chemistry, University of Bordeaux, Pessac, France. He has been a Director of this Institute from 2012 up to 2021. He is now a co-leader of the nationwide project DIADEM dedicated to Artificial Intelligence for Accelerated Materials Discovery. He has coauthored more than 250 papers and has been invited to 55 international conferences. His research interests are mostly concerned with the investigation of ferroelectric materials of any shape from single crystals to ceramics, nanocomposites and thin films.

Laurent Colin was born in Mortagne au Perche, France, in 1968. He received the technician degree in electronics and software in 1988. He worked at GIP Ultrasons (University of Tours) for the development of ultrasound systems for medical applications. Since 2017, he is an engineer at the CERTeM technological platform and GREMAN Laboratory (University of Tours). He works on instrumentation, characterization of ultrasonic transducers and sensors in particular cMUTs and high-frequency transducers.

Antoine Balé, photograph and biography not available at the time of publication.

Martin Flesch was born in Clamart in 1988. He received his Master's degree in Mechanical Engineering from ESCTA, Paris, France (2014). He obtained his Ph.D. degree from the Physics for Medicine Paris laboratory, ESPCI (Ecole Supérieure Physique Chimie Industrielles), Paris, France (2017). His doctoral research focused on studying ultrasound imaging solutions for real-time volumetric imaging. Currently, he serves as the Director of Innovation at Vermon, a manufacturer of ultrasound transducers and arrays for medical and industrial applications, located in Tours, France.

Franck Levassort (Member, IEEE) was born near Paris, France, in 1968. He received the bachelor's degree in applied physics and the D.E.A. (M.Sc.) degree in physical acoustics from University Paris 7-Denis Diderot, Paris, in 1990 and 1991, respectively, and the Ph.D. degree in ultrasound from the University of Tours, Tours, France, in 1996.

From 1997 to 2013, he was an Assistant Professor with the Institute of Technology, University of Tours, where he has been a Full Professor of electrical engineering since 2014. Since 2016, he has been the Deputy Director of GREMAN Laboratory, a joint research laboratory of more than 120 members on materials, microelectronics, acoustics, and nanotechnologies, University of Tours-CNRS-INSA CVL. His current research interests include the design, modeling, and characterization of piezoelectric composite materials and structures, and transducers for imaging applications.

Dr. Levassort is on the International Ultrasonic Symposium Technical Program Committee (Transducers and Transducer Materials).